Research Article | Vol. 25, No. 16 | 7 Aug 2017 | OPTICS EXPRESS 19094
Optics EXPRESS

Ultraslow weak-light solitons and their storage and retrieval in a kagome-structured hollow-core photonic crystal fiber

DATANG XU,[1] ZHIMING CHEN,[1,2] AND GUOXIANG HUANG[1,3,*]

[1]*State Key Laboratory of Precision Spectroscopy, School of Physical and Material Sciences, East China Normal University, Shanghai 200062, China*
[2]*School of Science, East China University of Technology, Nanchang 330013, China*
[3]*NYU-ECNU Joint Institute of Physics at NYU-Shanghai, Shanghai 200062, China*
[*]*gxhuang@phy.ecnu.edu.cn*

Abstract: We investigate the formation and propagation of ultraslow weak-light solitons and their memory in the atomic gas filled in a kagome-structured hollow-core photonic crystal fiber (HC-PCF) via electromagnetically induced transparency (EIT). We show that, due to the strong light-atom coupling contributed by the transverse confinement of the HC-PCF, the EIT and hence the optical Kerr nonlinearity of the system can be largely enhanced, and hence optical solitons with very short formation distance, ultraslow propagation velocity, and extremely low generation power can be realized. We also show that the optical solitons obtained can not only be robust during propagation, but also be stored and retrieved with high efficiency through the switching off and on of a control laser field. The results reported herein are promising for practical applications of all-optical information processing and transmission via the ultraslow weak-light solitons and the kagome-structured HC-PCF.

OCIS codes: (020.1670) Coherent optical effects; (190.5530) Pulse propagation and temporal solitons; (060.4370) Nonlinear optics, fibers.

References and links

1. M. Fleischhauer, A. Imamoglu, and J. P. Marangos, "Electromagnetically induced transparency: Optics in coherent media," Rev. Mod. Phys. **77**, 633 (2005).
2. J. B. Khurgin and R. S. Tucker (editors), *Slow Light: Science and Applications* (CRC, Taylor and Francis, Boca Raton, 2009).
3. Y. Wu and L. Deng, "Ultraslow Optical Solitons in a Cold Four-State Medium," Phys. Rev. Lett. **93**, 143904 (2004).
4. G. Huang, L. Deng, and M. G. Payne, "Dynamics of ultraslow optical solitons in a cold three-state atomic system," Phys. Rev. E **72**, 016617 (2005).
5. T. Hong, "Spatial Weak-Light Solitons in an Electromagnetically Induced Nonlinear Waveguide," Phys. Rev. Lett **90**, 183901 (2003).
6. M. Fleischhauer and M. D. Lukin, "Dark-State Polaritons in Electromagnetically Induced Transparency," Phys. Rev. Lett. **84**, 5094 (2000).
7. C. Simon, M. Afzelius, J. Appe, A. B. Giroday, S. J. Dewhurst, N. Gisin, C. Hu, F. Jelezko, S. Krąğoll, J. Mąğuler, J. Nunn, E. Polzik, J. Rarity, H. Riedmatten, W. Rosenfeld, A. J. Shields, N. Skąğold, R. M. Stevenson, R. Thew, I. Walmsley, M. Weber, H. Weinfurter, J. Wrachtrup, R. J. Young, "Quantum memories," Euro. Phys. J. D. **58**, 1 (2010).
8. A. I. Lvovsky, B. C. Sanders, W. Tittel, "Optical quantum memory," Nat. Photon. **3**, 706 (2009).
9. N. Sangouard, C. Simon, H. de Riedmatten, and N. Gisin, "Quantum repeaters based on atomic ensembles and linear optics," Rev. Mod. Phys. **83**, 33 (2011).
10. I. Novikova, R. L. Walsworth and Y. Xiao, "Electromagnetically induced transparency-based slow and stored light in warm atoms," Laser Photon. Rev. **6**, 333 (2012).
11. Y. Chen, Z. Bai, and G. Huang, "Ultraslow optical solitons and their storage and retrieval in an ultracold ladder-type atomic system," Phys. Rev. A **89**, 023835 (2014).
12. F. Benabid, J. C. Knight, G. Antonopoulos, and P. St. J. Russell, "Stimulated Raman scattering in Hydrogen-filled hollow-core photonic crystal fiber," Science **298**, 399 (2002).
13. F. Couny, F. Benabid, and P. S. Light, "Large-pitch kagome-structured hollow-core photonic crystal fiber," Opt. Lett. **31**, 3574 (2006).
14. G. J. Pearce, G. S. Wiederhecker, C. G. Poulton, S. Burger, and P. St. J. Russell, "Models for guidance in kagome-structured hollow-core photonic crystal fibres," Opt. Express **15**, 12680 (2007).

#292889 https://doi.org/10.1364/OE.25.019094
Journal © 2017 Received 14 Apr 2017; revised 9 Jul 2017; accepted 21 Jul 2017; published 31 Jul 2017

Optics EXPRESS

15. F. Benabid and P. J. Roberts, "Linear and nonlinear optical properties of hollow core photonic crystal fiber," J. Mod. Opt. **58**, 87 (2011).
16. P. St. J. Russell, P. Hölzer, W. Chang, A. Abdolvand, and J. C. Travers, "Hollow-core photonic crystal fibres for gas-based nonlinear optics," Nat. Photon. **8**, 278 (2014).
17. A. R. Bhagwat and A. L. Gaeta, "Nonlinear optics in hollow-core photonic bandgap fibers," Opt. Express **16**, 5035 (2008).
18. F. Benabid, P. S. Light, F. Couny, and P. St. J. Russell, "Electromagnetically-induced transparency grid in acetylene-filled hollow-core PCF," Opt. Express **13**, 5694 (2005).
19. S. Ghosh, A. R. Bhagwat, A. L. Gaeta, and B. J. Kirby, "Low-light-level optical interactions with Rubidium vapor in a photonic band-gap fiber," Phys. Rev. Lett. **97**, 023603 (2006).
20. P. S. Light, F. Benabid, F. Couny, M. Maric, and A. N. Luiten, "Electromagnetically induced transparency in Rb-filled coated hollow-core photonic crystal fiber," Opt. Lett. **32**, 1323 (2007).
21. M. Bajcsy, S. Hofferberth, V. Balic, T. Peyronel, M. Hafezi, A. S. Zibrov, V. Vuletic, and M. D. Lukin, "Efficient all-optical switching using slow light within a hollow fiber," Phys. Rev. Lett. **102**, 203902 (2009).
22. P. Londero, V. Venkataraman, A. R. Bhagwat, A. D. Slepkov, A. L. and Gaeta, "Ultralow-power four-wave mixing with Rb in a hollow-core photonic band-gap fiber," Phys. Rev. Lett. **103**, 043602 (2009).
23. P. S. Light, F. Benabid, G. J. Pearce, F. Couny, and D. M. Bird, "Electromagnetically induced transparency in acetylene molecules with counterpropagating beams in V and Λ schemes," Appl. Phys. Lett. **94**, 141103 (2009).
24. K. Saha, V. Venkataraman, P. Londero, and A. L. Gaeta, "Enhanced two-photon absorption in a hollow-core photonic-band-gap fiber," Phys. Rev. A **83**, 033833 (2011).
25. F. Blatt, L. S. Simeonov, T. Halfmann, and T. Peters, "Stationary light pulses and narrowband light storage in a laser-cooled ensemble loaded into a hollow-core fiber," Phys. Rev. A. **94**, 043833 (2016).
26. M. Facão, S. Rodrigues, and M. I. Carvalho, "Temporal dissipative solitons in a three-level atomic medium confined in a photonic-band-gap fiber," Phys. Rev. A **91**, 013828 (2015).
27. F. Benabid, J. C. Knight, and P. St. J. Russell, "Particle levitation and guidance in hollow-core photonic crystal fiber," Opt. Express **10**, 1195 (2002).
28. D. A. Steck, *Cesium D Line Data*, http://steck.us/alkalidata/.
29. J. Xu and G. Huang, "Electromagnetically induced transparency and ultraslow optical solitons in a coherent atomic gas filled in a slot waveguide," Opt. Express **21**, 5149 (2013).
30. L. Li, C. Zhu, L. Deng, and G. Huang, "Electromagnetically induced transparency and nonlinear pulse propagation in an atomic medium confined in a waveguide," J. Opt. Soc. Am. B **30**, 197 (2013).
31. Y. O. Dudin, L. Li, and A. Kuzmich, "Light storage on the time scale of a minute," Phys. Rev. A **87**, 031801(R) (2013).
32. R. W. Boyd, *Nonlinear Optics*, 3rd ed. (Academic, Elsevier, 2008).
33. M. R. Sprague, P. S. Michelberger, T. F. M. Champion, D. G. England, J. Nunn, X.-M. Jin, W. S. Kolthammer, A. Abdolvand, P. St. J. Russell, and I. A. Walmsley, "Broadband single-photon-level memory in a hollow-core photonic crystal fibre," Nat. Photon. **8**, 287 (2014).
34. The frequency and wavenumber of the signal field are given by $\omega_s + \Delta\omega$ and $k_s + K(\Delta\omega)$, respectively. $\Delta\omega$ $[K(\Delta\omega)]$ is the deviation of the signal-field frequency (wavenumber) when the atoms are present in the fiber core. Thus the point $\Delta\omega = 0$ corresponds to the center frequency of the signal field.
35. M. Graf, E. Arimondo, "Doppler broadening and collisional relaxation effects in a lasing-without-inversion experiment," Phys. Rev. A. **51**, 4030 (1995).
36. M. Bajcsy, S. Hofferberth, T. Peyronel, V. Balic, Q. Liang, A. S. Zibrov, V. Vuletic, and M. D. Lukin, "Laser-cooled atoms inside a hollow-core photonic-crystal fiber," Phys. Rev. A **83**, 063830 (2011).
37. C. Perrella, P. S. Light, T. M. Stace, F. Benabid, and A. N. Luiten, "High-resolution optical spectroscopy in a hollow-core photonic crystal fiber," Phys. Rev. A. **85**, 012518 (2012).
38. G. P. Agrawal, *Nonlinear Fiber Optics* (4th Edition) (Elsevier, 2007).
39. The Kerr nonlinearity in the HC-PCF in the absence of the atomic gas is many orders of magnitude smaller than the one obatined in the presence of the atomic gas via EIT given here, and hence can be neglected safely.
40. A. C. Newell and J. V. Moloney, *Nonlinear Optics* (Addison-Wesley, CA, 1992), Chap. 5.
41. C. Liu, Z. Dutton, C. Behroozi, and L. Hau, "Observation of coherent optical information storage in an atomic medium using halted light pulses," Nature **409**, 490 (2001).
42. D. F. Phillips, A. Fleischhauer, A. Mair, R. L. Walsworth, and M. D. Lukin, "Storage of Light in Atomic Vapor," Phys. Rev. Lett. **86**, 783 (2001).
43. I. Novikova, A. V. Gorshkov, D. F. Phillips, A. S. Sørensen, M. D. Lukin, and R. L. Walsworth, "Optimal control of light pulse storage and retrieval," Phys. Rev. Lett. **98**, 243602 (2007).
44. U. Schnorrberger, J. D. Thompson, S. Trotzky, R. Pugatch, N. Davidson, S. Kuhr, and I. Bloch, "Electromagnetically Induced Transparency and Light Storage in an Atomic Mott Insulator," Phys. Rev. Lett. **103**, 033003 (2009).
45. R. Zhao, Y. O. Dudin, S. D. Jenkins, C. J. Campbel, D. N. Matsukevich, T. A. B. Kennedy, and A. Kuzmich, "Long-lived quantum memory," Nat. Phys. **5**, 100 (2009).
46. R. Zhang, S. R. Garner, and L. V. Hau, "Creation of Long-Term Coherent Optical Memory via Controlled Nonlinear Interactions in Bose-Einstein Condensates," Phys. Rev. Lett. **103**, 233602 (2009).
47. A. G. Radnaev, Y. O. Dudin, R. Zhao, H. H. Jen, S. D. Jenkins, A. Kuzmich, and T. A. B. Kennedy, "A quantum

Optics EXPRESS

memory with telecom-wavelength conversion," Nat. Phys. **6**, 894 (2010).
48. Y. O. Dudin, R. Zhao, T. A. B. Kennedy, and A. Kuzmich, "Light storage in a magnetically dressed optical lattice," Phys. Rev. A **81**, 041805(R) (2010).
49. F. Yang, T. Mandel, C. Lutz, Z. S. Yuan, and J. W. Pan, "Transverse mode revival of a light-compensated quantum memory," Phys. Rev. A **83**, 063420 (2011).
50. H. N. Dai, H. Zhang, S. J. Yang, T. M. Zhao, J. Rui, Y. J. Deng, L. Li, N. L. Liu, S. Chen, X. H. Bao, X. M. Jin, B. Zhao, and J. W. Pan, "Holographic Storage of Biphoton Entanglement," Phys. Rev. Lett. **108**, 210501 (2012).
51. Y. H. Chen, M. J. Lee, I. C. Wang, S. Du, Y. F. Chen, Y. C. Chen, and I. A. Yu, "Coherent Optical Memory with High Storage Efficiency and Large Fractional Delay," Phys. Rev. Lett. **110**, 083601 (2013).
52. I. Novikova, N. B. Phillips, and A. V. Gorshkov, "Optimal light storage with full pulse-shape control," Phys. Rev. A **78**, 021802 (2008).
53. A. Eilam, A. D. Wilson Gordon, and H. Friedmann, "Efficient light storage in a Λ system due to coupling between lower levels," Opt. Lett. **34**, 1834 (2009).
54. G. Epple, K. S. Kleinbach, T. G. Euser, N. Y. Joly, T. Pfau, P. St. J. Russell, and R. Löw, "Rydberg atoms in hollow-core photonic crystal fibres," Nat. Commun. **5**, 4132 (2014).
55. C. Veit, G. Epple, H. Kübler, T. G. Euser, P. St. J. Russell, and R. Löw, "RF-dressed Rydberg atoms in hollow-core fibres," J. Phys. B: At. Mol. Opt. Phys. **49**, 134005 (2016).
56. The spatial length of the signal pulse in the propagation direction is given by $\tilde{V}_g\tau_0$, which is about 2.5 mm according to the result (12) and the pulse duration $\tau_0 = 1.0 \times 10^{-7}$ s.
57. J. C. Knight, I. Broeng, T. A. Birks, and P. St. J. Russell, "Photonic band gap guidance in optical fibers," Science **282**, 1476 (1998).
58. J. C. Travers, W. Chang, J. Nold, N. Y. Joly, and P. St. J. Russell, "Ultrafast nonlinear optics in gas-filled hollow-core photonic crystal fibers," J. Opt. Soc. Am. B. **28**, A11 (2011)
59. P. St. J. Russell, "Photonic crystal fibers," Science **299**, 358 (2003).
60. P. S. Light, F. Benabid, and F. Couny, "Electromagnetically induced transparency in Rb-filled coated hollow-core photonic crystal fiber," Opt. Lett. **32**, 1323 (2007).
61. N. V. Wheeler, M. D. W. Grogan, P. S. Light, F. Couny, T. A. Birks, and F. Benabid, "Large-core acetylene-filled photonic microcells made by tapering a hollow-core photonic crystal fiber," Opt. Lett. **35**, 1875 (2010).

1. Introduction

In recent years, tremendous efforts have been paid to the investigation on optical pulse memory, which is important for the realization of fast optical information processing. One of the main techniques to realize optical pulse memory is the utilization of electromagnetically induced transparency (EIT) [1,2], an interesting quantum interference effect typically occurring in three-level atomic systems. EIT can be used not only to cancel optical absorption in resonant quantum systems, but also to bring many novel nonlinear optical effects at weak-light level, including the production of weak-light solitons [3–5]. Based on the dark-state polariton [6] inherent in EIT systems, a signal optical mode can be mapped into an atomic mode, stored temporarily, and then retrieved from atoms by switching off and on of a control laser field [7–10].

However, nearly all researches reported up to now on the storage and retrieval of optical pulses via EIT are limited within linear optical regime. Due to the significant dispersion inherent in resonant systems, linear optical pulses in EIT-based atomic ensembles are not stable, resulting in a serious deformation for retrieved pulses and hence the loss of optical information. For practical applications of light memory, it is desirable to obtain a signal pulse that is robust not only during propagation, but also during storage and retrieval, and hence to acquire high efficiency and fidelity.

Recently, the EIT-based memory has been generalized to weak nonlinear optical regime, where the storage and retrieval of optical soliton pulses have been analyzed [11]. Nevertheless, because the optical pulses and atomic gases considered in Refs. [11] work in free space, the diffraction effect in those systems can not be neglected, which makes the optical soliton pulses unstable during propagation as well as during storage and retrieval. In addition, a larger power is needed for generating the optical soliton pulses in those systems since the coupling between light and atoms is weak in free space.

In this article, we propose a scheme for the formation, propagation, storage and retrieval of the optical soliton pulses in an atomic gas filled in a kagome-structured hollow-core photonic

Optics EXPRESS

crystal fiber (HC-PCF) [12–16] via EIT. Because of the transverse confinement provided by the fiber, the diffraction effect of the optical pulses is completely eliminated. We show that the EIT and hence the Kerr nonlinearity may be largely enhanced, which can be used to balance the dispersion and hence supports the production of the optical soliton pulses in the system. We prove that the optical soliton pulses obtained with such a scheme have very short formation distance (< 2 cm), ultraslow propagation velocity ($\sim 10^{-5}\,c$), and extremely low generation power ($\sim$ nW); in addition, they are robust during propagation and can be stored and retrieved with high efficiency through the switching on and off of a control laser field. The results reported here are promising for practical applications of all-optical information processing and transmission.

Before preceding, we note that bandgap-structured HC-PCFs [15–17] can also be used to perform EIT (see Refs. [18–25]), and to form an optical soliton pulse as shown recently by Facão *et al.* [26] where the fiber-core diameter is less than $4\,\mu$m. However, the use of the kagome-structured HC-PCF possesses many advantages, including: (i) The kagome-structured HC-PCF has a large core diameter ($26\,\mu$m-$100\,\mu$m in our scheme), which is easier not only for fabrication and but also for loading more atoms in the fiber core; (ii) Because of the larger atomic number in the kagome-structured HC-PCF, the coupling between the light field and the atomic gas is stronger, which is desirable for forming optical solitons within a shorter distance and with a lower generation power. (iii) Comparing with bandgap-structured HC-PCFs, the kagome-structured HC-PCF has a larger transverse transit time for the atoms in the fiber core, which admits a smaller dephasing and hence a higher efficiency for the storage and retrieval of the optical soliton pulses (see a further discussion in Sec. 5).

The rest of the article is arranged as follows. In Sec. II, the theoretical model is described. In Sec. III, the formation and propagation of ultraslow weak-light solitons is investigated. In Sec. 4, the storage and retrieval of optical soliton pulses are studied. Finally, in Sec. IV a discussion and a summary on the main results obtained in this work is given.

2. Model

We consider a pulsed signal laser field $\mathbf{E}_s$ and a continuous-wave (CW) control laser field $\mathbf{E}_c$, both are guided inside a kagome-structured HC-PCF with (hollow) core radius r_0 and pitch Λ_0 [Fig. 1(a)]. The core of the HC-PCF is filled with an atomic gas with a lambda-type level configuration [Fig. 1(b)]. In the absence of the atomic gas, the HC-PCF allows many eigenmodes of electric field $\mathbf{E}$ with the form $\mathbf{e}_\alpha\, q_\alpha(x,y)\, \exp\{i[\beta_\alpha(\omega)z-\omega t]\}$, here $\mathbf{e}_\alpha$, $q_\alpha(x,y)$, and β_α are the polarization unit vector, eigenfunction, and propagation constant for the mode with index α (for a simple introduction of the eigenmodes in the kagome-structured HC-PCF, see Appendix A). In the present study, we are interested in the fundamental mode of the HC-PCF made of silica. The blue solid line in Fig. 1(c) is the numerical result of the electric-field distribution in the radius direction (with $r \equiv \sqrt{x^2+y^2}$ the radius coordinate of the system) of the fundamental mode for $r_0 = \Lambda_0 = 13\,\mu$m when the atomic gas is absent. The shape of the fundamental mode can be fitted well by the zeroth-order Bessel function [27] [the red dashed curve in Fig. 1(c)]. One sees that the fundamental mode is well confined in the fiber core, as shown in the inset of Fig. 1(c). In Fig 1(b), $|1\rangle$, $|2\rangle$, and $|3\rangle$ are respectively the metastable, ground, and excited states, Δ_3 and Δ_2 are respectively one- and two-photon detunings, Γ_{jl} ($j=1,2$; $l=3$) denotes the spontaneous emission rate from $|l\rangle$ to $|j\rangle$; ω_s and Ω_s [ω_c and Ω_c] are respectively the angular and half Rabi frequencies of the signal (control) field, which is coupled to the transition $|1\rangle \leftrightarrow |3\rangle$ ($|2\rangle \leftrightarrow |3\rangle$). Both of the signal and control fields belong to the fundamental mode of the HC-PCF and propagate along z direction, with the form $\mathbf{E} = \mathbf{E}_s + \mathbf{E}_c = \sum_{l=s,c} \mathbf{e}_l \sqrt{\frac{\hbar\omega_l}{2\epsilon_0 V_l^{\rm eff}}}\mathcal{E}_l(z,t) q_l(x,y)\, e^{i[\beta_l z-\omega_l t]} + \text{c.c.}$, where $\beta_l \equiv \beta(\omega_l)$, $V_l^{\rm eff} \equiv L_z \iint |q_l(x,y)|^2 dxdy$ is the effective mode volume for the mode $\omega = \omega_l$, L_z is the

Optics EXPRESS

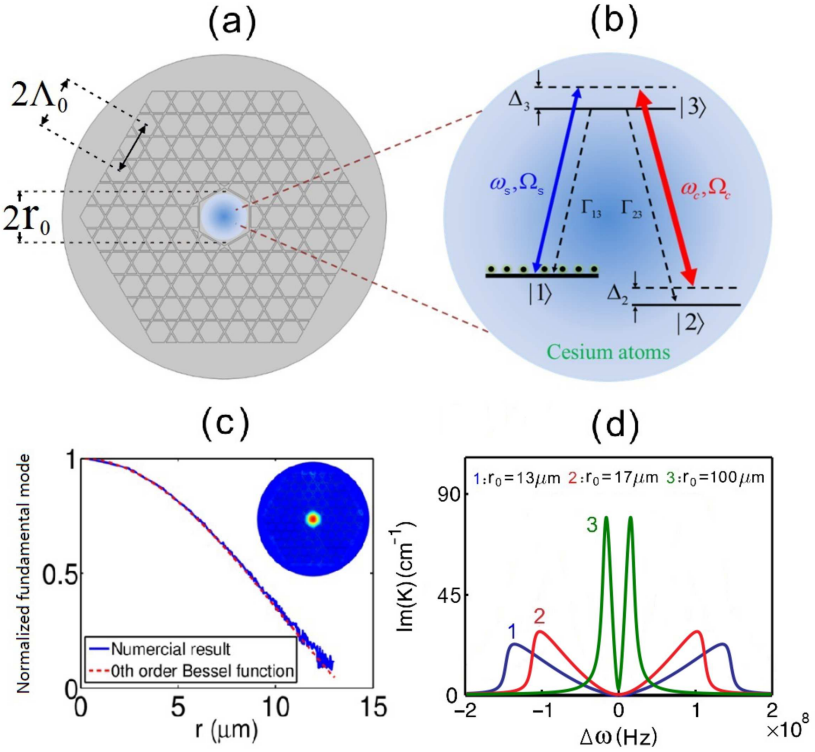

Fig. 1. (a) Kagome-structured HC-PCF with core radius r_0 and pitch Λ_0. (b) Atoms of a lambda-type three-level configuration are filled within the hollow core of the fiber, and initially prepared in the metastable $|1\rangle$ for suppressing four-wave mixing effect. (c) Numerical result of the electric-field distribution of the normalized fundamental-mode amplitude as a function of radius coordinate r in the HC-PCF made of silica when the atoms are absent. (d) Absorption spectrum Im(K) of the signal field as a function of $\Delta\omega$ for different core radius r_0. The red, blue and green lines are for $r_0 = 13\,\mu$m, $17\,\mu$m, and $100\,\mu$m, respectively. The other notations in the figure are explained in the text.

fiber length, the subscript s (c) denotes the signal (control) field, and c.c. represents complex conjugate.

We choose a cesium atomic gas with the energy levels selected as $|1\rangle = |6^2S_{1/2}, F = 4\rangle$, $|2\rangle = |6^2S_{1/2}, F = 3\rangle$, and $|3\rangle = |6^2P_{3/2}, F = 4\rangle$. For such level configuration the wavelengths of the signal and control fields are approximately equal (i.e. $\lambda_s \approx \lambda_c = 852\,$nm) [28], which means $q_c(x, y) \approx q_s(x, y) \equiv q(x, y)$. For an analytical description, in the following the fundamental mode is approximated by the zero-order Bessel function $q(x, y) = J_0(kr)$ when $r \leq r_0$ and $q(x, y) = 0$ when $r > r_0$ with $k \approx 2.405/r_0$ [27], which gives $V_c^{\rm eff} \approx V_s^{\rm eff} = \pi r_0^2 J_1^2(kr_0) L_z \equiv V^{\rm eff}$. In order to have a quantitative discussion on light-beam confinement effect in the HC-PCF, following the approach in Refs. [29, 30] we define a reference mode volume of free space, i.e. $V^{\rm ref} = \pi R_\perp^2 L_z$. The quantity $R_\perp$ (determined by input condition) is the transverse radius of laser beams in free space, introduced here for illustrating the confinement effect due to the HC-PCF by comparing the EIT in the HC-PCF and the EIT in free space. Note that experimentally $R_\perp$ is usually large (e.g., $R_\perp = 100\,\mu$m [31], which is chosen in the following discussion). Then the electric field can be expressed as

$$\mathbf{E} = \sum_{l=s,c} \mathbf{e}_l \frac{R_\perp}{r_0 J_1(kr_0)} \mathcal{E}_l(z,t) q_l(x,y)\, e^{i[\beta_l z - \omega_l t]} + \text{c.c.}. \tag{1}$$

Optics EXPRESS

When the atomic gas is filled into the fiber, under electric-dipole and rotating-wave approximations, the Hamiltonian of the system in the interaction picture reads $\hat{H}_{\rm int} = -\hbar\sum_{j=1}^{3}\Delta_j|j\rangle\langle j| - \hbar[\zeta(x,y)\Omega_s|1\rangle\langle 3| + \zeta(x,y)\Omega_c|2\rangle\langle 3| + \text{h.c.}]$, where $\zeta(x,y) \equiv \frac{R_\perp}{r_0 J_1(kr_0)}q(x,y)$, and $\Omega_s = |\mathbf{p}_{13}|\mathcal{E}_s/\hbar$ ($\Omega_c = |\mathbf{p}_{23}|\mathcal{E}_c/\hbar$) is the half Rabi frequency of the signal (control) field, with $\mathbf{p}_{jl}$ the electric-dipole moment associated with the state $|j\rangle$ and the state $|l\rangle$. The equation of motion for the density matrix σ in the interaction picture reads [32]

$$i\hbar\left(\frac{\partial}{\partial t} + \Gamma\right)\sigma = \left[\hat{H}_{\rm int}, \sigma\right], \tag{2}$$

where σ is a 3×3 density matrix with matrix elements $\sigma_{jl} \equiv |j\rangle\langle l|$, Γ is a 3×3 relaxation matrix denoting the spontaneous emission and dephasing. The explicit expression of Eq. (2) is presented in Appendix B.

The equation of motion for Ω_s can be obtained by the Maxwell equation $\nabla^2\mathbf{E} - (1/c^2)\partial^2\mathbf{E}/\partial t^2 = [1/(\epsilon_0 c^2)]\partial^2\mathbf{P}_p/\partial t^2$, with the electric polarization intensity given by $\mathbf{P}_p = \mathbf{P}_{\rm host} + \mathcal{N}\mathbf{p}_{13}\sigma_{31}\exp[i(\beta_s z - \omega_s t)] + \text{c.c.}$, where $\mathcal{N}$ is the atomic density, $\mathbf{P}_{\rm host} = \epsilon_0\chi_{\rm host}\mathbf{E}$ is the electric polarization intensity, with $\chi_{\rm host} = \chi_{\rm host}(x,y)$ is the susceptibility of HC-PCF in the absence of the atomic gas. According to the expression of the electric field [i.e. the Eq. (1)] and using Eq. (18), the Maxwell equation under a slowly varying envelope approximation is reduced to

$$i\left(\frac{\partial}{\partial z} + \frac{\langle n^2\rangle}{cn_{\rm eff}}\frac{\partial}{\partial t}\right)\Omega_s + \kappa_{13}\langle\tilde{\sigma}_{31}\rangle = 0, \tag{3}$$

where $n \equiv [1+\chi_{\rm host}(x,y)]^{1/2}$ is the refractive index [$\chi_{\rm host}(x,y)$ is the electric susceptibility] of the HC-PCF in the absence of the atomic gas, $\kappa_{13} \equiv \mathcal{N}\omega_s|\mathbf{p}_{13}|^2/(2\hbar\epsilon_0 c n_{\rm eff})$ is light-atom coupling coefficient with $n_{\rm eff}$ the effective refractive index. In Eq. (3) we have defined $\sigma_{31} = \tilde{\sigma}_{31}\zeta(x,y)$ and $\langle\psi\rangle = \iint|\zeta(x,y)|^2\psi(x,y)dxdy/\iint|\zeta(x,y)|^2dxdy$, with ψ an arbitrary function of x and y (for the detailed derivation of Eq. (3), see Appendix A). We see that, the diffraction effect of the signal field is effectively canceled due to the transverse (mode) confinement of the HC-PCF.

For simplicity, the following assumptions are made for our theoretical calculations presented below: (i) To suppress Doppler effect, the atoms are assumed to be cooled to low temperature and the signal and the control fields are injected with opposite directions. (ii) To reduce the dephasing rate caused by the adsorption of atoms to the inner walls of the fiber core, the inner walls are coated with some materials, or a light-induced atomic desorption process is used to release the atoms into the center of fiber core, or a dipole trap along the fiber axis is employed to attract the atoms away from the inner walls of the fiber. (iii) The atoms are initially populated on the metastable state $|1\rangle$ by an optical pumping to suppress four-wave mixing effect. These assumptions are realistic because related experiments have already been done in recent years [19, 21, 33].

3. Ultraslow weak-light solitons in the HC-PCF

3.1. Linear dispersion relation and EIT enhancement

We first solve the Maxwell-Bloch (MB) equations (2) and (3) in the linear regime and discuss the linear property of the system. The steady state before the signal field opens is $\sigma_{11} = 1$ and all other σ_{jl} are zero. When the signal field is switched on but very weak, the system will evolve into a time-dependent state and the solution of the MB equations (2) and (3) have the solution $\sigma_{11} = 1$, $\sigma_{j1} \sim \exp(i\theta)$ ($j = 2, 3$), $\Omega_s \sim \exp(i\theta)$, and $\sigma_{22} = \sigma_{33} = \sigma_{32} = 0$, with $\theta = K(\Delta\omega)z - \Delta\omega t$ [34]. The linear dispersion relation is given by

$$K = \frac{\Delta\omega}{c}\frac{\langle n^2\rangle}{n_{\rm eff}} + \kappa_{13}\left\langle\frac{(\Delta\omega + d_{21})}{|\zeta(x,y)\Omega_c|^2 - (\Delta\omega + d_{21})(\Delta\omega + d_{31})}\right\rangle, \tag{4}$$

here the definitions of the parameters d_{21} and d_{31} have been given in Appendix B. Because the signal field is resonant with the atoms in the fiber, in usual cases one expects that a significant absorption will happen. However, the absorption can be made very low in the present system. Fig. 1(d) shows the calculation result on the imaginary part of K, i.e. Im(K), as a function of $\Delta\omega$, where the blue, red and green lines are respectively for the core radius $r_0 = 13\,\mu$m, $17\,\mu$m, and $100\,\mu$m. From Fig. 1(d) we see that: (i) A transparency window (i.e., the dip near $\Delta\omega = 0$) is opened, which is due to the quantum interference (i.e. EIT) effect induced by the control field; (ii) For different core radius r_0, the width of the transparency window (called EIT transparency window) is different. The smaller the value of r_0, the wider the EIT transparency window, which means that the EIT effect is enhanced when the core radius r_0 is reduced. The physical reason of the enhancement of EIT effect is due to the existence of the (geometrical) confinement effect in the kagome-structured HC-PCF. By the confinement, the control field Ω_c has an enhanced factor $(R_\perp/r_0)[J_1(kr_0)]^{-1}$, which leads to a larger EIT transparency window for smaller r_0. For instance, the transparency window is very wide for $r_0 = 13\,\mu$m, which will be used in our following calculations.

When plotting Fig. 1(d), the system parameters are chosen as $\Omega_c = 1.0 \times 10^7$ s^{-1}, $\Delta_2 = \Delta_3 = 0$, $|\mathbf{p}_{13}| \simeq |\mathbf{p}_{23}| = 3.8 \times 10^{-27}$ C$\cdot$cm [28], $\mathcal{N} = 2.0 \times 10^{10}$ cm^{-3}, $R_\perp = 100\ \mu$m, $\Gamma_3 \simeq 2\gamma_{31} = \pi \times 5.23$ MHz, $\gamma_{31} = \gamma_{32}$. Note that the ground-state dephasing rate $\gamma_{21}^{\rm dep}$ for the atoms filled in the HC-PCF may be caused by many physical factors, widely discussed in literature (see, e.g., [18, 20, 25, 35–37]). Here we take $\gamma_{21}^{\rm dep} = \gamma_{21} \simeq 2\pi \times 0.05$ MHz in our numerical calculations carried out here and below, which is slightly larger than that given in the recent experiment [25] in order to account for the factors causing the dephasing not included in our model.

3.2. Nonlinear envelope equation

The approach above is valid not only for CW but also for pulsed signal fields. However, vanishing one- and two-photon detunings assumed there usually cannot be satisfied in reality, which will result in a dispersion effect in the system and hence the spreading of the signal pulse. In particular, in light memory what we need is to store and retrieve a signal pulse within a finite time duration. The sideband components of the pulse are detuned from the energy-level difference of the related transition ($|1\rangle$ to $|3\rangle$ in the present system), which brings a non-negligible dispersion effect to the system. Such effect brings not only a deformation of the signal pulse but also a reduction of the quality of light memory in the system.

In order to suppress the dispersion effect and obtain a shape-preserving signal pulse useful for light memory, one can exploit the Kerr effect of the system to balance the dispersion [3, 4]. In fact, the Kerr nonlinearity of the system can be largely enhanced in the present system by both the EIT effect and the confinement effect of the HC-PCF, as shown below.

To this end, based on the MB equations (2) and (3) we derive a nonlinear envelope equation describing the nonlinear evolution of the signal field by using the method developed in Ref. [4]. Taking the asymptotic expansion $\sigma_{jk} = \sum_{l=0}^{\infty} \epsilon^l \sigma_{jk}^{(l)}$ (j, k =1, 2, 3; $\sigma_{jk}^{(0)} = \delta_{j1}\delta_{k1}$), and $\Omega_s = \sum_{l=1}^{\infty} \epsilon^l \Omega_s^{(l)}$. Here ϵ is a dimensionless small parameter characterizing the typical amplitude of the signal pulse. All the quantities on the right-hand side of the expansion are considered as functions of the multi-scale variables $z_l = \epsilon^l z$ ($l = 0, 1, 2, \cdots$) and $t_l = \epsilon^l t$ ($l = 0, 1, 2, \cdots$). Substituting the expansions into the Eqs. (2) and (3) and comparing the coefficients of ϵ^m (m=1, 2, 3), we obtain a set of linear but inhomogeneous equations which can be solved order by order.

The first-order ($m = 1$) solution is given by

$$\Omega_s^{(1)} = F\,\exp(i\theta), \tag{5a}$$

$$\sigma_{j1}^{(1)} = \frac{\delta_{j3}(\Delta\omega + d_{21}) - \delta_{j2}\zeta^*(x,y)\Omega_c^*}{|\zeta(x,y)\Omega_c|^2 - (\Delta\omega + d_{21})(\Delta\omega + d_{31})}\zeta(x,y)Fe^{i\theta}, \quad (j = 2, 3) \tag{5b}$$

Optics EXPRESS

with all other $\sigma_{jl}^{(1)} = 0$. Here $\theta \equiv K(\Delta\omega)z_0 - \Delta\omega t_0$, with F a yet to be determined envelope function depending on the indicated slow variables t_1, z_1, and z_2 and $K(\Delta\omega)$ the same as (4). At the second order ($m = 2$), we obtain the solvability condition i$[\partial F/\partial z_1 + (\partial K/\partial\Delta\omega)\partial F/\partial t_1] = 0$, which shows that the signal-pulse envelope F travels with the group velocity $V_g \equiv K_1^{-1} = (\partial K/\partial\Delta\omega)^{-1}$, given by

$$V_g = \left\{ \frac{1}{c}\frac{\langle n^2 \rangle}{n_{\rm eff}} + \kappa_{13} \left\langle \frac{(\Delta\omega + d_{21})^2 + |\zeta(x,y)\Omega_c|^2}{[|\zeta(x,y)\Omega_c|^2 - (\Delta\omega + d_{21})(\Delta\omega + d_{31})]^2} \right\rangle \right\}^{-1}. \tag{6}$$

The explicit expressions of the second-order approximation solutions are given in Appendix C.

With the above results we go to the third order ($m = 3$). A solvability condition in this order yields the equation for the signal-pulse envelope $i\partial F/\partial z_2 - (1/2)[\partial^2 K/\partial\Delta\omega^2]\,\partial^2 F/\partial t_1^2 - W|F|^2 F e^{-2\bar{a}z_2} = 0$, here $K_2 \equiv \partial^2 K/\partial\Delta\omega^2$ describes the second-order dispersion, and the nonlinear coefficient

$$W = -\kappa_{13} \left\langle \frac{\zeta(x,y)\Omega_c a_{32}^{*(2)} + (\Delta\omega + d_{21})(2a_{11}^{(2)} + a_{22}^{(2)})}{|\zeta(x,y)\Omega_c|^2 - (\Delta\omega + d_{21})(\Delta\omega + d_{31})} \right\rangle \tag{7}$$

is related to optical Kerr effect describing the self-phase modulation of the signal field.

Combining the solvability conditions in all orders and returning to the original variables, we obtain the equation

$$i\frac{\partial U}{\partial z} - \frac{K_2}{2}\frac{\partial^2 U}{\partial \tau^2} - W|U|^2 U = -iaU, \tag{8}$$

where $\tau = t - z/V_g$, $U = \epsilon F e^{-\bar{a}z_2}$, and $a = \epsilon^2\bar{a}$, with the definition of $\bar{a}$ presented in Appendix C. Note that Eq. (8) is valid for $\Delta\omega \ll \omega_s$. Since we are interested in the evolution of the signal pulse at the center frequency ω_s, in the calculations given below all the coefficients in Eq. (8) will be evaluated at $\Delta\omega = 0$.

3.3. Ultraslow weak-light solitons

The third-order nonlinear optical susceptibility $\chi^{(3)}$ of the signal field is proportional to the self-phase modulation coefficient W in Eq. (8) via the relation

$$\chi^{(3)} = \frac{2c}{\omega_s}\frac{|\mathbf{p}_{13}|^2}{\hbar^2}W. \tag{9}$$

Using the system parameters given in the last subsection but with $\Omega_c = 3.6 \times 10^6$ s^{-1}, $\Delta_2 = 2.5 \times 10^7$ s^{-1}, $\Delta_3 = 3.75 \times 10^8$ s^{-1}, $\mathcal{N} = 2.0 \times 10^{10}$ cm^{-3} and $r_0 = 13\,\mu$m, we obtain $W = (-5.38 + 0.16i) \times 10^{-13}$ cm^{-1} s^2 and Re$(\chi^{(3)}) = -1.56 \times 10^{-2}$ cm^2 V^{-2}, which is many orders of magnitude larger than that in conventional fibers [38]. Hence the HC-PCF with the filled atomic gas via EIT possesses greatly enhanced Kerr nonlinearity [39], contributed from the quantum interference effect in the (resonant) atomic gas, which is very useful for practical applications of many nonlinear optical processes, including effective four-wave mixing and formation of weak-light solitons.

Since the system under study is a resonant one, the coefficients in Eq. (8) are generally complex. However, when the system works under the EIT condition, the absorption of the signal field can be largely suppressed, and therefore the imaginary part of these coefficients can be made to be much smaller. Thus Eq. (8), when writing into the dimensionless form, can be approximated by the nonlinear Schrödinger equation $i\partial u/\partial s + \partial^2 u/\partial\sigma^2 + 2|u|^2 u = 0$, where $u = U/U_0$, $s = -z/(2L_D)$, and $\sigma = \tau/\tau_0$, with $L_D = \tau_0^2/\tilde{K}_2$ (τ_0 is the pulse duration of the signal field) the typical dispersion length of the system. Note that we have taken

Optics EXPRESS

$L_N = L_D$ with $L_N = 1/(\tilde{W}U_0^2)$ the typical nonlinear length, and thus $U_0 = (1/\tau_0)\sqrt{\tilde{K}_2/\tilde{W}}$ (typical Rabi frequency of the signal field in free space). Here the tilde above K_2 and W means taking the real part, $\tilde{K}_2 = \mathrm{Re}(K_2)$ and $\tilde{W} = \mathrm{Re}(W)$. A single-soliton solution reads $u(s,\sigma) = 2\vartheta \mathrm{sech}[2\vartheta(\sigma - \sigma_0 + 4\delta s)] \exp[-2i\delta\sigma - 4i(\delta^2 - \vartheta^2)s - i\phi_0]$, where ϑ, σ_0, δ, and ϕ_0 are real free parameters that determine the amplitude (also width), propagating velocity, initial position, and initial phase of the soliton, respectively. For simplicity, we take $\vartheta = 1/2$, $\sigma_0 = \delta = \phi_0 = 0$. Then, when returning to original variables, we obtain the expression of the signal field $\mathbf{E}_s = \mathbf{e}_s E_s$, with

$$\begin{aligned} E_s &= \frac{\hbar}{\tau_0|\mathbf{p}_{13}|}\sqrt{\frac{\tilde{K}_2}{\tilde{W}}}\frac{R_\perp}{r_0 J_1(kr_0)} J_0\left(2.405\frac{r}{r_0}\right)\mathrm{sech}\left[\frac{1}{\tau_0}\left(t - \frac{z}{\tilde{V}_g}\right)\right] \\ &\quad \times \exp\left[i\left(\tilde{K}_0 - \frac{1}{2L_D}\right)z - i(\omega_s + \Delta\omega)t\right] + \mathrm{c.c.}, \end{aligned} \tag{10}$$

here $\tilde{K}_0 \equiv \mathrm{Re}(K_0)$, with $K_0 = K(\Delta\omega)|_{\Delta\omega=0}$.

We now give a set of system parameter for the formation of the optical soliton given above. By taking $\Omega_c = 3.6 \times 10^6$ s^{-1}, $\tau_0 = 1.0 \times 10^{-7}$ s, $\Delta_2 = 2.5 \times 10^7$ s^{-1}, $\Delta_3 = 3.75 \times 10^8$ s^{-1}, $\mathcal{N} = 2.0 \times 10^{10}$ cm^{-3} and other parameters are the same as those given in the above text, we obtain (evaluated at $\Delta\omega = 0$) $K_0 = (-3.23 + 0.09i)$ cm^{-1}, $K_1 = (4.05 - 0.33i) \times 10^{-8}$ cm^{-1} s, $K_2 = (-3.45 + 0.39i) \times 10^{-15}$ cm^{-1} s^2, $W = (-5.38 + 0.16i) \times 10^{-13}$ cm^{-1} s^2, $U_0 = 0.8 \times 10^6$ s^{-1}, and $L_A = 1/\mathrm{Im}(K_0) = 10.39$ cm (typical absorption length). In particular, the nonlinearity length of the system is given by

$$L_N = 2.9 \text{ cm}, \tag{11}$$

which means that to form the soliton very short fiber length is needed. With these parameters we obtain

$$\tilde{V}_g = \mathrm{Re}(V_g) = 8.17 \times 10^{-4}\, c, \tag{12}$$

which means that the optical soliton has an ultraslow propagating velocity.

The energy flux of the ultraslow optical soliton in the HC-PCF predicted by Eq. (10) can be calculated by using the Poynting vector integrated over the hollow core cross-section, i.e., $P = \iint dxdy(\mathbf{E}_s \times \mathbf{H}_s) \cdot \mathbf{e}_z$, where $\mathbf{e}_z$ is the unit vector in the propagation direction [40]. At leading order the corresponding magnetic field of the soliton, $\mathbf{H}_s$, is transverse and in the $\mathbf{e}_s \times \mathbf{e}_z$ direction. Thus if $\mathbf{e}_s = \mathbf{e}_y$ then $\mathbf{H}_s = \mathbf{e}_x H_s$ with $H_s \approx n_{\mathrm{eff}}\epsilon_0 c E_s$. After averaging over the carrier-wave period, we obtain $P = P_{\max}\,\mathrm{sech}^2\left[\left(t - z/\tilde{V}_g\right)/\tau_0\right]$, where $P_{\max} = 2\epsilon_0 c n_{\mathrm{eff}}(\hbar U_0/|\mathbf{p}_{13}|)^2 \iint |\zeta(x,y)|^2 dxdy$, with n_{eff} the effective refractive index of the signal field, given in the Appendix A [i.e. Fig. (6)]. Using the parameters given above, we obtain

$$P_{\max} = 0.82 \times 10^{-9}\,\mathrm{W}, \tag{13}$$

i.e., the optical soliton has extremely low generation power. We see that, very different from the optical solitons obtained in conventional solid-core optical fibers [38], the optical soliton presented here has many attractive characters, including the very short formation distance [given by (11)], the ultra slow propagation velocity [given by (12)], and the extremely low generation power [given by (13)]. Physical reasons for these characters come from the enhanced EIT and Kerr nonlinear effects in the resonant atomic gas confined in the core of the kagome-structured HC-PCF.

Shown in Fig. 2(a) is the propagation of the ultraslow optical soliton with $|\Omega_s(z,\tau)\tau_0|$ as a function of z/L_D and t/τ_0. The comparison of waveshapes at $z = 0$ and at $z = 2L_D$ is given

Optics EXPRESS

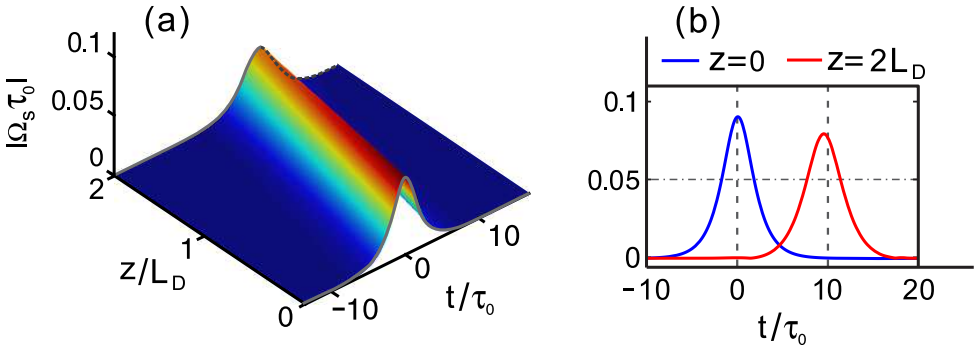

Fig. 2. (a) The propagation of the ultraslow optical soliton, with $|\Omega_s(z,\tau)\tau_0|$ as a function of z/L_D and t/τ_0 (L_D is dispersion length and τ_0 is pulse duration). (b) The comparison of waveshapes between $z=0$ (blue curve) and $z=2L_D$ (red curve).

by Fig. 2(b). The solution is obtained by numerically solving Eq. (8) with all the imaginary parts of the complex coefficients taken into account. In the simulation, the initial condition is chosen as $\Omega_s(0,\tau)\tau_0 = 0.08\,\mathrm{sech}(t/\tau_0)$. One sees that, although due to the dissipative effect (mainly contributed by the dephsing $\gamma_{21}^{\mathrm{dep}}$) there is a weak amplitude decay when propagating to $z=2L_D$, the soliton can keep its shape well for a propagation distance up to $2L_D = 5.8\,\mathrm{cm}$.

4. Storage and retrieval of the ultraslow weak-light solitons in kagome structured HC-PCF

4.1. *Storage and retrieval of the optical soliton pulse in a small-core kagome-structured HC-PCF*

Although many schemes have been proposed and realized in the atomic gases in free space (see Refs. [41–51] and references therein), the light memory using an atomic gas filled in HC-PCFs is more desirable. The reasons are the following. First, guided-wave optics can confine optical modes within a small area over a distance longer than that is possible with diffractive optics in free space, thus the light power required to obtain strong light-atom coupling can be largely reduced, which can increase light memory efficiency. Second, an integrated platform is easier to interface with existing photonic architectures and also easier to scale up. Thus it is nature to seek the possibility of the storage and retrieval of the ultraslow weak-light solitons obtained in the last section.

The principle of EIT-based light memory is as follows [6]. When switching on the control field, the signal pulse propagates in the atomic gas with nearly vanishing absorption; by slowly switching off the control field the signal pulse disappears and gets stored in the atomic gas in the form of atomic coherence; when the control field is switched on again the signal pulse appears again. However, this principle was usually applied for linear optical pulses, which are not stable during propagation and suffer serious deformation due to the dispersion and/or diffraction. In the following, we show that it is available to realize the memory of stable optical soliton pulses in the kagome-structured HC-PCF obtained in the last section.

To this end, we numerically solve the MB equations (2) and (3) by taking the control field to be adiabatically changed with time to realize the function of its switching on and off. The switching-on and the switching-off of the control field are modeled by the combination of two hyperbolic tangent functions with the form

$$\Omega_c = \Omega_{c0}\left\{1 - \frac{1}{2}\tanh\left[\frac{t-T_c^{\mathrm{off}}}{T_s}\right] + \frac{1}{2}\tanh\left[\frac{t-T_c^{\mathrm{on}}}{T_s}\right]\right\}, \tag{14}$$

Optics EXPRESS

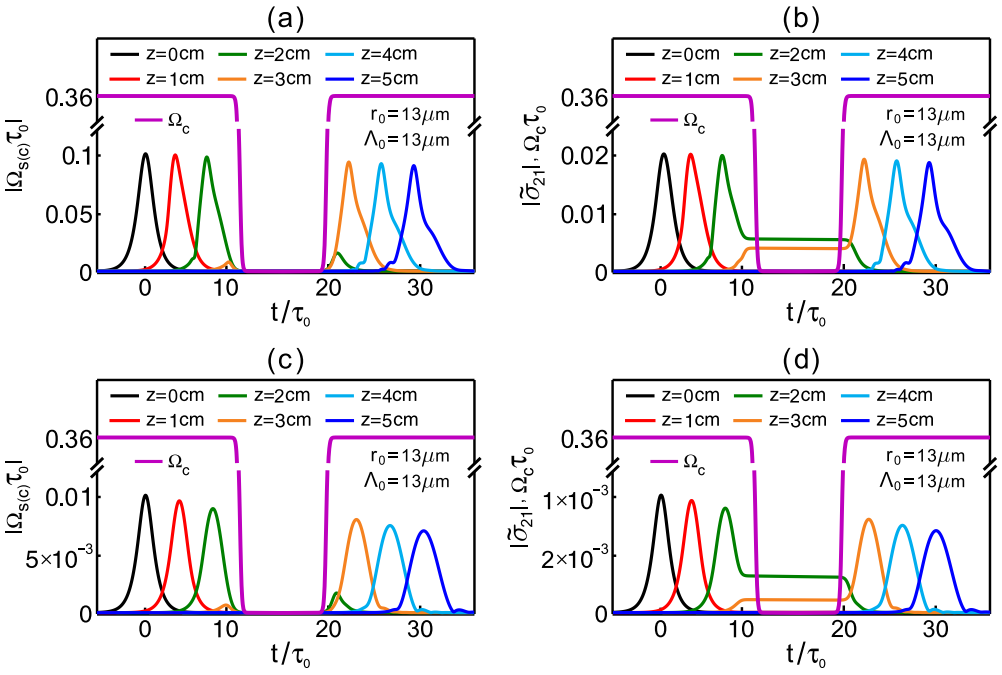

Fig. 3. Numerical results on the storage and retrieval of an optical soliton pulse and a linear optical pulse for $r_0 = \Lambda_0 = 13\,\mu$m. (a) [(b)] Evolution of the dimensionless half Rabi frequency $|\Omega_s\tau_0|$ of the signal field (atomic coherence $\tilde{\sigma}_{21}$) as a function of time t for different propagation distance z in the soliton regime. (c) [(d)] Evolution of the dimensionless half Rabi frequency $|\Omega_s\tau_0|$ of the signal field (atomic coherence $\tilde{\sigma}_{21}$) as a function of t for different z in the linear regime. In each panel, the black, red, green, yellow, sky blue, and blue solid lines are for z=0, 1, 2, 3, 4 and 5 cm, respectively; the purple solid line represents the dimensionless half Rabi frequency $|\Omega_c\tau_0|$ of the control field.

where $T_c^{\rm off}$ and $T_c^{\rm on}$ are respectively the times of switching-off and switching-on of the control field. The switching time of the control field is T_s and the storage time of the signal pulse is approximately given by $T_c^{\rm on} - T_c^{\rm off}$. We choose $T_s = 0.5\tau_0$, $T_c^{\rm off} = 10.0\tau_0$, $T_c^{\rm on} = 20.0\tau_0$, with $\tau_0 = 1.0 \times 10^{-7}$ s. Note that due to the light confinement in the transverse directions, the MB equations [i.e. (2) and (3)] controlling the motion of the atoms filled in the HC-PCF are different from those in free space. In particular, the mode function $\zeta(x, y)$ appears in the coefficients of these equations, making the calculation of light memory more complicated than that in free space.

We first consider the kagome-structured HC-PCF with a relatively small core radius r_0 (but much larger than that of the bandgap-structured HC-PCF in Ref. [26]). In this case, the system can be well approximated by a quasi-one-dimensional waveguide since the variation of the electric field on x and y is much faster than that on z, and hence the light memory can be studied by using the Eq. (3) and effective Bloch equation (23) (see Appendixes B and D). Shown in Fig. 3(a) is the result of storage and retrieval of an optical soliton pulse for $r_0 = \Lambda_0 = 13\,\mu$m, where $|\Omega_s\tau_0|$ is taken as a function of the propagation distance z and the evolution time t. The wave shape of the input signal pulse is taken as a hyperbolic secant one with a larger amplitude for forming soliton, i.e., $\Omega_s^{\rm in}(t)\tau_0 = 0.1\,{\rm sech}(1.5t/\tau_0)$. The black, red, green, yellow, sky blue, and blue solid lines in each panel are for the soliton pulse propagating to the distance z=0, 1, 2, 3, 4 and 5 cm, respectively; the purple solid line is for the dimensionless half Rabi frequency $|\Omega_c\tau_0|$ of the control field. From the figure, we see that in this soliton regime the pulse is narrowed (i.e. the soliton is indeed formed) before its storage because of the balance

Optics EXPRESS

between the dispersion and nonlinearity in the system. When the control field is switched off at $t = T_c^{\rm off} = 10\,\tau_0$, the soliton pulse disappears, and then appears again when the control field is switched on at $t = T_c^{\rm on} = 20\,\tau_0$.

During the storage stage, the energy (information) of the optical soliton pulse is transferred into the atomic gas. Fig. 3(b) shows the result of the atomic coherence $|\tilde{\sigma}_{21}|$ as a function of z and t. One sees that $\tilde{\sigma}_{21}$ is nonzero during the switch-off of the control field. Since the signal pulse is stored in the form of atomic coherence $\tilde{\sigma}_{21}$ when the control field is switched off and is retained until the control field is switched on again, the atomic coherence $\tilde{\sigma}_{21}$ can be taken as the intermediary for the memory of the signal pulse.

The efficiency η of the light memory can be described by the energy ratio between the retrieved pulse and the input pulse [52], i.e.,

$$\eta = \frac{\int_{T_c^{\rm on}}^{\infty} dt \iint_{r\le r_0} dxdy\,|E_s^{\rm out}(x,y,t)|^2}{\int_{-\infty}^{T_c^{\rm off}} dt \iint_{r\le r_0} dxdy\,|E_s^{\rm in}(x,y,t)|^2}, \tag{15}$$

where $E_s^{\rm in}(x,y,t) = E_s(x,y,z,t)|_{z=0}$ and $E_s^{\rm out}(x,y,t) = E_s(x,y,z,t)|_{z=L_z}$, with L_z the fiber length. Our calculation gives that the optical pulse memory efficiency in this soliton regime is $\eta = 86.3\%$ for $L_z = 5\,$cm. The fidelity of the light memory can be characterized by the quantity ηJ^2, here J^2 is the overlap integral

$$J^2 = \frac{|\int_{-\infty}^{T_c^{\rm off}} dt \iint_{r\le r_0} dxdy\,E_s^{\rm out}(x,y,t+\Delta T)E_s^{\rm in}(x,y,t)|^2}{\int_{-\infty}^{T_c^{\rm off}} dt \iint_{r\le r_0} dxdy\,|E_s^{\rm in}(x,y,t)|^2 \cdot \int_{T_c^{\rm on}}^{\infty} dt \iint_{r\le r_0} dxdy\,|E_s^{\rm out}(x,y,t)|^2}, \tag{16}$$

where ΔT is the time interval between the peak of the input signal pulse $E_s^{\rm in}$ and the peak of the retrieved signal pulse $E_s^{\rm out}$. From Fig. 3(a) we see that the peak of the input signal pulse (the black solid curve) is at $t = 0$ and the peak of the retrieved signal pulse (the blue solid curve) is at $t = 28\tau_0$, and hence $\Delta T = 28\tau_0$. Using the formula (16) we obtain $J^2 = 91.9\%$ for $L_z = 5\,$cm. Thus, the fidelity of the optical soliton memory is $\eta J^2 = 79.4\%$.

For comparison, the optical pulse memory in a linear regime is also calculated. Fig. 3(c) shows the result of numerical simulation on the evolution of $|\Omega_s\tau_0|$ as function of z and t. The input signal pulse is also taken as a hyperbolic secant function but with a much smaller amplitude, i.e., $\Omega_s^{\rm in}(t)\tau_0 = 0.01\,{\rm sech}(1.5t/\tau_0)$. The colored solid lines are for z=0, 1, 2, 3, 4 and 5 cm, respectively. At beginning, the pulse profile for red line ($z = 1\,$cm) in Fig. 3(b) is similar to that in Fig. 3(a) with almost same peak amplitude and pulse width. However, after 5 cm propagation, the peak value of blue line ($z = 5\,$cm) decreases to 6.8×10^4 and its width is more than $2.0\tau_0$. The blue line in Fig. 3(a) still keeps its amplitude and pulse width. From the figure, we see that the retrieved signal pulse is significantly broadened and its amplitude decreases rapidly. Based on Eqs. (15) and (16), we obtain the memory efficiency and fidelity of the linear optical pulse, respectively given by $\eta = 79.8\%$ and $\eta J^2 = 62.9\%$ for $L_z = 5\,$cm, lower than the optical soliton memory shown in Fig. 3(a). The atomic coherence $|\tilde{\sigma}_{21}|$ of the linear optical pulse during the storage and retrieval is presented in Fig. 3(d).

For a given storage time, the memory efficiency of the optical soliton pulse depends on the fiber length L_z and the fiber core radius r_0 when the other system parameters are fixed. Fig. 4 shows the result of η as a function of the fiber length L_z for the storage time $T_c^{\rm on} - T_c^{\rm off} = 10\tau_0$. The blue, red and green solid curves in the figure are respectively for r_0 taking 13, 15, and 17 μm (the pitch Λ_0 is fixed to be 13 μm). From the figure we can obtain the following conclusions: (i) For any core radius r_0, the memory efficiency η grows rapidly in the small L_z region (i.e. the region on the left side of its peak value), then as L_z increases it reaches to the peak value, and finally drops down slowly in the large L_z region (i.e. the region on the right side of the peak value); (ii) In the large (small) L_z region, the smaller the core radius r_0 the higher (lower) the

Optics EXPRESS

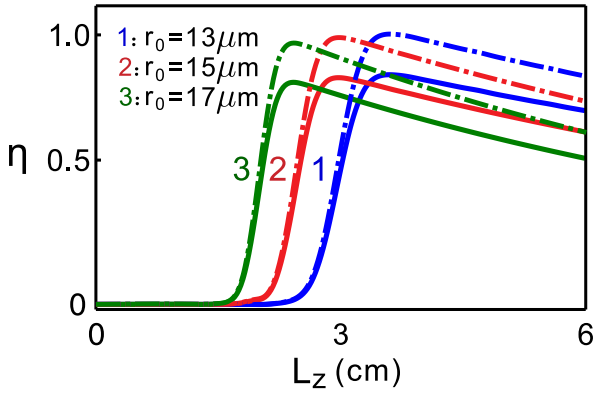

Fig. 4. Memory efficiency η of the optical soliton pulse as a function of the fiber length L_z. Solid lines are fitted curves based on numerical calculation. The blue, red and green solid lines are for the fiber core radius r_0=13, 15 and 17 μm, respectively. Dashed-dotted lines for each core radius are the memory efficiencies when a microwave field is coupled to the two lower atomic levels [i.e. $|1\rangle$ and $|2\rangle$ in Fig. 1(b)].

memory efficiency η. The physical reasons are the following. Since the signal pulse in the fiber with a larger core radius has a smaller group velocity, in the small L_z region (where damping due to the spontaneous emission and dephasing is negligible) the compression of the signal pulse is more effective and hence the memory efficiency for the large-core fiber is larger than that of the small-core fiber. However, in the large L_z region (where damping plays a significant role), the attenuation of the signal pulse in the small-core fiber is relatively smaller than in the large-core fiber and thus the memory efficiency is higher for the small-core fiber. Consequently, one can acquire a large memory efficiency of the optical soliton pulse by suitably selecting the core radius and the fiber length.

The main factor affecting the light memory efficiency and fidelity is the value of the dephasing rate $\gamma_{21}^{\rm dep}$. To improve the efficiency and fidelity, one can employ a microwave field to couple the two lower atomic levels [i.e. $|1\rangle$ and $|2\rangle$ in Fig. 1(b)]. The microwave field is applied within the time interval in which the control field is switched off, which can provide a gain to the atomic coherence σ_{21} [53]. We have carried out a numerical simulation on the memory of an optical soliton pulse by adding such a microwave field into the system, with the result shown by the dashed-dotted lines in Fig. 4. We see that by using the microwave field the soliton memory efficiency can be increased by 20%, which is valid for the all values of the core-radius r_0.

4.2. *Storage and retrieval of the optical soliton pulse for a large-core kagome-structured HC-PCF*

As pointed out previously, a large-core fiber is desirable to fill more atoms in its core to obtain a strong light-atom coupling in the system. Recently, the core radius r_0 of kagome-structured HC-PCF has been extended to 50 μm [54, 55], which encourages us to consider the memory of optical soliton pulse with such large-core fiber.

To this end, we make a numerical simulation to investigate the memory of optical soliton pulse in a kagome-structured HC-PCF with the core radius $r_0 = 50\,\mu$m and the pitch $\Lambda_0 = 25\,\mu$m. Note that in this situation the distribution range of the mode function $\zeta(x, y)$ is relatively large, the effective Bloch equation [i.e. Eq. (23)] is not a good approximation. Nevertheless, the (reduced) Maxwell equation (3) is still valid since the distribution range of $\zeta(x, y)$ is still much smaller than the spatial length of the signal pulse in the propagation (i.e. z) direction [56]. Thus the simulation is carried out based on the Eqs. (3) and (19).

Shown in Fig. 5(a) is the result of the storage and retrieval of an optical soliton pulse in the

Optics EXPRESS

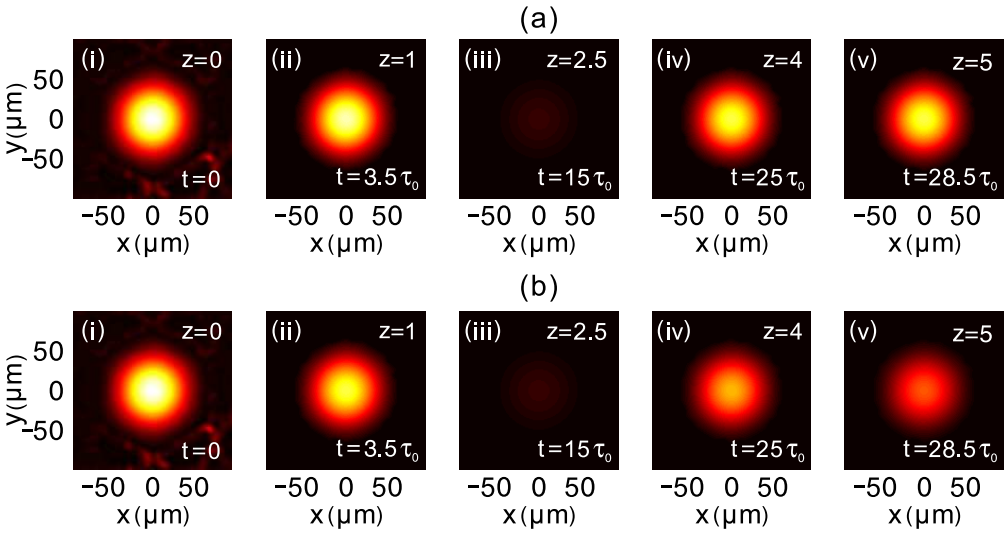

Fig. 5. (a) Storage and retrieval of the optical soliton pulse in the HC-PCF with core radius $r_0 = 50$ μm and pitch $\Lambda_0 = 25\,\mu$m. The subplots from (i) to (v) give the intensity distribution $|E_s|^2$ of the soliton pulse in the (x, y) plane when propagating to the distance $z = 0$, 1, 2.5, 4, and 5 cm, respectively. $t = 0$, $3.5\tau_0$, $15\tau_0$, $25\tau_0$, and $28.5\tau_0$ shown respectively in (i) to (v) are the times when soliton's peak arrives at the positions $z = 0$, 1, 2.5, 4, and 5 cm, respectively. (b) Storage and retrieval of a linear optical pulse in the same fiber.

large-core fiber. The switching on and off of the control field is still modeled by the function (14). Panels (i) to (v) in the figure give the electric-field intensity distribution $|E_s|^2$ of the soliton pulse in the (x, y) plane for the soliton propagating to the distance $z = 0$, 1, 2.5, 4, and 5 cm, respectively. $t = 0$, $3.5\tau_0$, $15\tau_0$, $25\tau_0$, and $28.5\tau_0$ shown respectively in (i) to (v) are the times when the peak of the soliton arrives at the positions $z = 0$, 1, 2.5, 4, and 5 cm, respectively. We see that the optical soliton pulse can still be stored and retrieved in the system and can keep well its shape during the storage process. The efficiency and fidelity of the light memory in the present case are $\eta = 77.6\%$ and $\eta J^2 = 71.2\%$ for $L_z = 5$ cm, respectively.

For comparison, Fig. 5(b) shows the storage and retrieval of a linear optical pulse in the same large-core fiber. One sees that during the storage process the linear optical pulse undergoes a significant decrease of the amplitude. By the formulas (15) and (16) one obtains small memory efficiency ($\eta = 63.8\%$) and small fidelity ($\eta J^2 = 50.3\%$), lower than the optical soliton memory shown in Fig. 5(a).

5. Discussion and summary

From the results described above, we see that the optical soliton pulses in the kagome-structured HC-PCF can not only be robust during propagation, but also be stored and retrieved with relatively higher efficiency and fidelity.

We note that there are two types of HC-PCFs, i.e., bandgap-structured HC-PCFs and kagome-structured HC-PCFs [15–17, 57–59]. The bandgap-structured HC-PCFs have a true bandgap for eigenfrequency, which can be taken as a guidance mechanism preventing light from propagating in fibre cladding and confining the light within the fiber core. The EIT and related phenomena based on such HC-PCFs were demonstrated in many previous studies (see, e.g., Refs. [18–25]). The kagome-structured HC-PCFs do not possess a bandgap, so the light is guided by different mechanisms (e.g., anti-resonant reflection) [15]. The EIT and related Raman memory based on such HC-PCFs were also reported [33, 60, 61].

Optics EXPRESS

Our work presented above is different from that considered in Ref. [26], where the authors employed a bandgap-structured HC-PCF with a small core radius and did not discuss the storage and retrieval of optical solitons. In contrast, in our work not only the formation and propagation but also the storage and retrieval of the optical solitons are investigated, both are based on the kagome HC-PCF. In addition, our work is also at variance with those studied in Refs. [18–25, 33, 60, 61], where no optical solitons and their storage and retrieval were studied. We stress that the light memory using the atomic gas filling into the kagome HC-PCF has higher efficiency and fidelity than those using an atomic gas in free space. For comparison, consider the same cesium atomic gas (used above) works in a free space with the same control field Ω_c. If the input signal pulse has the transverse mode profile $q(x, y) = J_0(kr)$, the characteristic diffraction length of the system reads $L_{Dif} = \sqrt{3}\pi r_0^2/\lambda_s$. If $r_0 = 13\,\mu$m ($r_0 = 50\,\mu$m), one has $L_{Dif} = 0.1\,$cm ($L_{Dif} = 1.6\,$cm), which is much shorter than the medium length (5 cm) and thus the diffraction effect in the system is very significant. Due to the diffraction, the signal pulse spreads fast in the transverse directions and its amplitude decreases rapidly. As a result, one obtains, for $r_0 = 13\,\mu$m ($r_0 = 50\,\mu$m), the light memory efficiency and fidelity are respectively given by $\eta = 0.997\%$ and $\eta J^2 = 0.786\%$ ($\eta = 16.65\%$ and $\eta J^2 = 14.39\%$), which are much lower than those obtained by using the kagome-structured HC-PCF considered above.

Note that in principle one can take bandgap-structured HC-PCFs [15–17] for generating the ultraslow weak-light soliton pulses and for realizing their storage and retrieval. However, the kagome-structured HC-PCFs, as indicated in Sec. 1, are better for implementing such tasks. For instance, using the core radius $r_0 = 5\,\mu$m and the atomic density $\mathcal{N} = 3.0 \times 10^9\ \text{cm}^{-3}$ in the bandgap-structured HC-PCF given in Ref. [21], under the same control field one obtains the nonlinear coefficient describing Kerr effect [defined by (9)] $W = (5.05 + 0.31i) \times 10^{-16}\ \text{cm}^{-1}\ \text{s}^2$ and hence the nonlinearity length (describing the formation distance of the optical solitons) $L_N = 8.62\,$cm. Nevertheless, using the core radius $r_0 = 13\,\mu$m and $\mathcal{N} = 1.1 \times 10^{11}\ \text{cm}^{-3}$ in the kagome-structured HC-PCF given in Ref. [33], one obtains $W = (2.17 + 0.44i) \times 10^{-14}\ \text{cm}^{-1}\ \text{s}^2$ and hence $L_N = 0.3\,$cm. Thus, comparing with the bandgap-structured HC-PCF, the Kerr effect in the kagome-structured HC-PCF can be made much larger, and hence the formation distance of the optical soliton pulses can be made much smaller, which is desirable for generating the solitons with a lower power and a smaller system size. In addition, due to the longer L_N and larger dephasing caused by larger transverse transit time, the memory efficiency of the soliton storage in the bandgap-structured HC-PCF is less than 22%, much lower than that in the kagome-structured HC-PCF ($> 77\%$). Due to these reasons, the kagome-structured HC-PCF is chosen in our model. We expect that the result and method reported herein will be useful not only for the understanding of nonlinear optical property of gas-filled HC PCFs, but also for practical applications for manipulating optical information at weak-light level.

In summary, in this work we have investigated the formation and propagation of ultraslow weak-light solitons and their memory in cold atomic gas filled in a kagome-structured HC-PCF via EIT. We have shown that, due to the strong light-atom coupling provided by the transverse confinement of the HC-PCF, the EIT and thus the Kerr nonlinearity of such system can be largely enhanced. As a result, stable optical solitons with ultralow generation power down to nW and the propagation velocity slow to $10^{-5}\,c$ can be realized. We have demonstrated that the optical solitons obtained can not only be robust during propagation, but also be stored and retrieved with high memory efficiency and fidelity through the switching off and on of a control laser field. The energy to generate soliton signals in HC-PCF is very low thus it is possible to realize such light memory in weak nonlinear regime under single photon level. The results reported herein are promising for practical applications of optical information processing and transmission based on the ultraslow weak-light solitons and kagome-structured HC-PCFs.

Optics EXPRESS

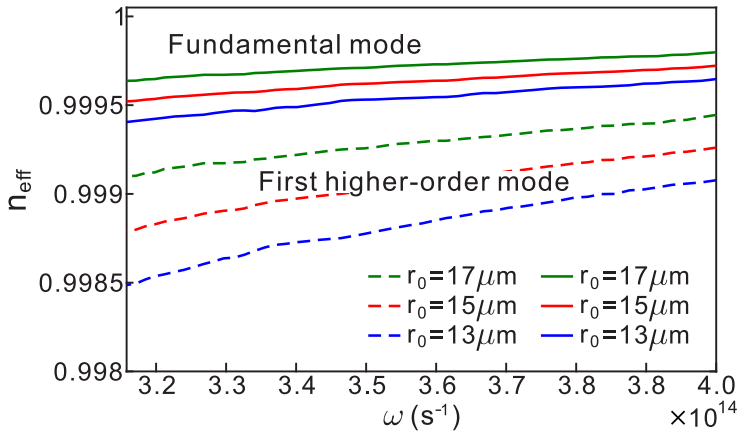

Fig. 6. Numerical result for the effective refractive index $n_{\rm eff}$ of the kagome-structured HC-PCF as a function of frequency ω with pitch $\Lambda_0 = 13$ μm and three different core radius r_0. The solid (dashed) line is for the fundamental (first higher-order) mode; the blue, red, and green colors are for $r_0 = 13$ μm, $r_0 = 15$ μm, $r_0 = 17$ μm, respectively.

Appendix

A. Electric-field mode functions of the kagome-structured HC-PCF

When in the absence of the atomic gas, the electric field $\mathbf{E}$ of the kagome-structured HC-PCF satisfies the Maxwell equation $\nabla^2\mathbf{E} - (1/c^2)\partial^2\mathbf{E}/\partial t^2 = [1/(\epsilon_0 c^2)]\partial^2\mathbf{P}/\partial t^2$, here $\mathbf{P}$ is electric polarization intensity. Assuming that the frequency of $\mathbf{E}$ is far from the resonant frequency of the HC-PCF material, the electric polarization intensity has the from $\mathbf{P} = \epsilon_0\chi_{\rm host}(x,y)\mathbf{E}$, where $\chi_{\rm host}(x,y)$ is the electric susceptibility of the HC-PCF. Then the Maxwell equation is simplified into $\nabla^2\mathbf{E} - (n^2/c^2)\partial^2\mathbf{E}/\partial t^2 = 0$, with $n = n(x,y) = [1+\chi_{\rm host}(x,y)]^{1/2}$ the refractive index of the HC-PCF without the atomic gas.

The general solution of the Maxwell equation can be written as

$$\mathbf{E} = \sum_{\alpha}\sum_{\omega} \mathbf{e}_\alpha(\omega)\mathcal{E}_\alpha(\omega)\, q_\alpha(x,y)\, e^{i[\beta_\alpha(\omega)z-\omega t]} + \text{c.c.}, \tag{17}$$

where $\mathbf{e}_\alpha$, $\mathcal{E}_\alpha$, $q_\alpha(x,y)$, and β_α are the polarization unit vector, mode amplitude, eigenfunction, and propagation constant for the mode with index α. The eigenfunction q_α satisfies the equation

$$\left(\frac{\partial^2}{\partial x^2} + \frac{\partial^2}{\partial y^2}\right) q_\alpha(x,y) + \frac{n^2(x,y)\omega^2}{c^2} q_\alpha(x,y) = \beta_\alpha^2(\omega) q_\alpha(x,y). \tag{18}$$

Since an analytical solution of Eq. (18) is not available, we resort a numerical simulation. Shown in Fig. 6 is the numerical result for the effective refractive index $n_{\rm eff}(\omega)$ of the kagome-structured HC-PCF as a function of frequency ω. The solid (dashed) line is for the fundamental (first higher-order) mode; the blue, red, and green colors are for $r_0 = 13$ μm, $r_0 = 15$ μm, $r_0 = 17$ μm, respectively. In the calculation, we assume the fiber is made of silica and the pitch Λ_0 (defined by the distance between two adjacent holes) of the HC-PCF [see Fig. 1(a)] is fixed to be $\Lambda_0 = 13\,\mu$m. Form the figure we see that the first higher-order mode has a lower effective refractive index than the fundamental mode. Based on the effective refractive indexes obtained we can find the corresponding eigenfunctions.

We are interested in the fundamental mode, whose electric-field distribution in the radial direction (i.e. as a function of $r = \sqrt{x^2+y^2}$) is shown by the blue solid line in Fig. 1(c). When obtaining the figure, $r_0 = \Lambda_0 = 13\,\mu$m is chosen. The shape of the fundamental mode

Optics EXPRESS

can be fitted well by the zeroth-order Bessel function $J_0(2.405r/r_0)$ [the red dashed curve in Fig. 1(c)] [27]. One sees that the fundamental mode is well confined in the fiber core, as shown in the inset of Fig. 1(c).

B. Equations of motion for the density-matrix elements

The equation of motion for the density-matrix elements σ_{jl} reads [32]

$$i\frac{\partial}{\partial t}\sigma_{11} - i\Gamma_{13}\sigma_{33} + \zeta^*(x,y)\Omega_s^*\sigma_{31} - \zeta(x,y)\Omega_s\sigma_{31}^* = 0, \tag{19a}$$

$$i\frac{\partial}{\partial t}\sigma_{22} - i\Gamma_{23}\sigma_{33} + \zeta^*(x,y)\Omega_c^*\sigma_{32} - \zeta(x,y)\Omega_c\sigma_{32}^* = 0, \tag{19b}$$

$$i\frac{\partial}{\partial t}\sigma_{33} + i\Gamma_3\sigma_{33} - \zeta^*(x,y)\Omega_s^*\sigma_{31} + \zeta(x,y)\Omega_s\sigma_{31}^* - \zeta^*(x,y)\Omega_c^*\sigma_{32} + \zeta(x,y)\Omega_c\sigma_{32}^* = 0, \tag{19c}$$

$$\left(i\frac{\partial}{\partial t} + d_{21}\right)\sigma_{21} - \zeta(x,y)\Omega_s\sigma_{32}^* + \zeta^*(x,y)\Omega_c^*\sigma_{31} = 0, \tag{19d}$$

$$\left(i\frac{\partial}{\partial t} + d_{31}\right)\sigma_{31} - \zeta(x,y)\Omega_s(\sigma_{33} - \sigma_{11}) + \zeta(x,y)\Omega_c\sigma_{21} = 0, \tag{19e}$$

$$\left(i\frac{\partial}{\partial t} + d_{32}\right)\sigma_{32} - \zeta(x,y)\Omega_c(\sigma_{33} - \sigma_{22}) + \zeta(x,y)\Omega_s\sigma_{21}^* = 0, \tag{19f}$$

where $d_{jl} = \Delta_j - \Delta_l + i\gamma_{jl}$, $\Delta_3 = \omega_s - \omega_{31}$ and $\Delta_2 = \omega_{12} - (\omega_c - \omega_s)$ are respectively one- and two-photon detuings, with $\omega_{jl} = (E_j - E_l)/\hbar$ with E_j the eigenenergy of the state $|j\rangle$. The dephasing rates are defined as $\gamma_{jl} = (\Gamma_j + \Gamma_l)/2 + \gamma_{jl}^{\rm dep}$, with $\Gamma_j = \sum_{E_l<E_j}\Gamma_{lj}$ representing the rate of spontaneous emission of the state $|j\rangle$ to all lower energy states $|l\rangle$, and $\gamma_{jl}^{\rm dep}$ being the dephasing rate reflecting the loss of phase coherence between $|j\rangle$ and $|l\rangle$.

Under the slowly varying envelope approximation, the equation of motion for Ω_s reads

$$i\zeta(x,y)\left(\frac{\partial}{\partial z} + \frac{n^2}{cn_{\rm eff}}\frac{\partial}{\partial t}\right)\Omega_s + \kappa_{13}\sigma_{31} = 0, \tag{20}$$

with $n^2 = 1 + \chi_{\rm host}(x,y)$ the refractive index of the HC-PCF when the atomic gas is absent. When the spatial distribution range of $\zeta(x,y)$ is much smaller than in the spatial length of the signal pulse in the propagation (i.e. z) direction, by using the definition $\sigma_{31} = \tilde{\sigma}_{31}\zeta(x,y)$ and $\langle\psi\rangle = \iint|\zeta(x,y)|^2\psi(x,y)dxdy/\iint|\zeta(x,y)|^2dxdy$, Eq. (20) is reduced into Eq. (3) given in the main text.

C. Second-order approximation solution

The second-order approximation solution reads $\sigma_{21}^{(2)} = a_{21}^{(2)}i\frac{\partial}{\partial t_1}Fe^{i\theta}$, $\sigma_{31}^{(2)} = a_{31}^{(2)}i\frac{\partial}{\partial t_1}Fe^{i\theta}$, $\sigma_{jj}^{(2)} = a_{jj}^{(2)}|F|^2e^{-2\bar{a}z_2}$ $(j=1,2,3)$, $\sigma_{32}^{(2)} = a_{32}^{(2)}|F|^2e^{-2\bar{a}z_2}$, with $\bar{a} = \epsilon^{-2}{\rm Im}[K(\Delta\omega)|_{\Delta\omega=0}]$

Optics EXPRESS

and

$$a_{11}^{(2)} = \frac{P_2 - P_1}{-i\Gamma_{13}|\zeta(x,y)\Omega_c|^2\left(\frac{1}{d_{32}^*} - \frac{1}{d_{32}}\right)}|\zeta(x,y)|^2, \tag{21a}$$

$$a_{22}^{(2)} = \frac{G|\zeta(x,y)|^2 - i\Gamma_{13}a_{11}^{(2)}}{i\Gamma_{13}}, \tag{21b}$$

$$a_{21}^{(2)} = -\frac{\zeta^*(x,y)\Omega_c^*(2\Delta\omega + d_{21} + d_{31})}{D^2}\zeta(x,y), \tag{21c}$$

$$a_{31}^{(2)} = \frac{(\Delta\omega + d_{21})^2 + |\zeta(x,y)\Omega_c|^2}{D^2}\zeta(x,y), \tag{21d}$$

$$a_{32}^{(2)} = \frac{\zeta(x,y)\Omega_c}{d_{32}}[\frac{|\zeta(x,y)|^2}{D^*} - (a_{11}^{(2)} + 2a_{22}^{(2)})], \tag{21e}$$

where $P_1 = [i\Gamma_{23} - 2|\zeta(x,y)\Omega_c|^2(1/d_{32} - 1/d_{32}^*)]G$, $P_2 = i\Gamma_{13}|\zeta(x,y)\Omega_c|^2[1/(Dd_{32}^*) - 1/(D^*d_{32})]$, with $G = (\Delta\omega + d_{21}^*)/D^* - (\Delta\omega + d_{21})/D$ and $D = |\zeta(x,y)\Omega_c|^2 - (\Delta\omega + d_{21})(\Delta\omega + d_{31})$.

D. Effective Bloch equation

Making the transformation [40]

$$\tilde{\sigma}_{jj}(z,t) = \frac{\int_{-\infty}^{\infty} dxdy|\zeta(x,y)|^2\sigma_{jj}(x,y,z,t)}{\int_{-\infty}^{\infty} dxdy|\zeta(x,y)|^2}, \qquad (j = 1,2,3) \tag{22a}$$

$$\tilde{\sigma}_{21}(z,t) = \frac{\int_{-\infty}^{\infty} dxdy|\zeta(x,y)|^2\sigma_{21}(x,y,z,t)}{\int_{-\infty}^{\infty} dxdy|\zeta(x,y)|^2}, \tag{22b}$$

$$\tilde{\sigma}_{31(32)}(z,t)\,\zeta(x,y) = \sigma_{31(32)}(x,y,z,t), \tag{22c}$$

Eq. (19) is reduced into the effective Bloch equation

$$i\frac{\partial}{\partial t}\tilde{\sigma}_{11} - i\Gamma_{13}\tilde{\sigma}_{33} + \rho\Omega_s^*\tilde{\sigma}_{31} - \rho\Omega_s\tilde{\sigma}_{31}^* = 0, \tag{23a}$$

$$i\frac{\partial}{\partial t}\tilde{\sigma}_{22} - i\Gamma_{23}\tilde{\sigma}_{33} + \rho\Omega_c^*\tilde{\sigma}_{32} - \rho\Omega_c\tilde{\sigma}_{32}^* = 0, \tag{23b}$$

$$i\frac{\partial}{\partial t}\tilde{\sigma}_{33} + i\Gamma_3\tilde{\sigma}_{33} - \rho\Omega_s^*\tilde{\sigma}_{31} + \rho\Omega_s\tilde{\sigma}_{31}^* - \rho\Omega_c^*\tilde{\sigma}_{32} + \rho\Omega_c\tilde{\sigma}_{32}^* = 0, \tag{23c}$$

$$\left(i\frac{\partial}{\partial t} + d_{21}\right)\tilde{\sigma}_{21} - \rho\Omega_s\tilde{\sigma}_{32}^* + \rho\Omega_c^*\tilde{\sigma}_{31} = 0, \tag{23d}$$

$$\left(i\frac{\partial}{\partial t} + d_{31}\right)\tilde{\sigma}_{31} - \Omega_s(\tilde{\sigma}_{33} - \tilde{\sigma}_{11}) + \Omega_c\tilde{\sigma}_{21} = 0, \tag{23e}$$

$$\left(i\frac{\partial}{\partial t} + d_{32}\right)\tilde{\sigma}_{32} - \Omega_c(\tilde{\sigma}_{33} - \tilde{\sigma}_{22}) + \Omega_s\tilde{\sigma}_{21}^* = 0, \tag{23f}$$

with $\rho = \int_{-\infty}^{\infty} dxdy|\zeta(x,y)|^4 / \int_{-\infty}^{\infty} dxdy|\zeta(x,y)|^2$, describing the confinement of the HC-PCF in the transverse directions.

Funding

National Natural Science Foundation of China (No. 11474099) and Science & Technology Project of Department of Education of Jiangxi Province (No. GJJ160576).